npj | 2D materials and applications

Article

Published in partnership with FCT NOVA with the support of E-MRS

https://doi.org/10.1038/s41699-025-00639-0

# Chemical treatment-induced indirect-to-direct bandgap transition in $MoS_2$: impact on excitonic emission



Yusuf Kerem Bostan[1], Elanur Hut[1], Cem Sanga[2], Nadire Nayir[2,3], Ayse Erol[1], Yue Wang[4] ✉ & Fahrettin Sarcan[1,4] ✉

Effective doping is crucial for overcoming performance limitations in two-dimensional (2D) transition metal dichalcogenide (TMD) devices. For light-emitting applications, however, doping must increase carrier injection without quenching excitonic emission. While chemical treatment with 1,2-dichloroethane (DCE) has been demonstrated as an effective post-growth n-doping method for 2D TMDs, its effects on optical properties, specifically the retention of optical characteristics and excitonic behaviour, remain unclear. Here, we investigate the layer- and time-dependent optical effects of DCE on molybdenum disulfide ($MoS_2$) using photoluminescence (PL) spectroscopy and Density Functional Theory (DFT). Our results show that DCE treatment rapidly reduces the indirect bandgap transition, while leaving the direct transition unaffected. DFT confirms that chlorine atoms bind to sulphur vacancies, creating in-gap states that facilitate non-radiative recombination and suppress the indirect PL. This work demonstrates DCE can selectively engineer the optical band structure in $MoS_2$, paving the way for more efficient 2D optoelectronic devices.

Over the past decades, two-dimensional (2D) transition metal dichalcogenides (TMDs) have attracted significant attention due to their ultrathin structures, tuneable bandgaps, and excellent sensing capabilities[1–4]. Their atomically thin structure leads to high surface-to-volume ratios, making their electrical conductivity highly sensitive to environmental changes - a desirable characteristic for sensing applications[5]. Key examples of TMDs such as $WS_2$, $WSe_2$, $MoS_2$, and $MoTe_2$ are alternative active materials for optoelectronic devices, including LEDs and lasers, and their bandgaps, which can be precisely tuned via thickness, strain and doping[6–11], offering an additional degree of freedom to tailor their light-emitting properties. A unique feature of layered TMDs is their characteristic transition from an indirect to a direct bandgap in the monolayer limit, attributed to quantum confinement[12]. This is particularly beneficial for optoelectronic devices, as direct bandgaps allow efficient radiative recombination of electrons and holes without requiring phonon assistance, resulting in stronger light emission and absorption. Despite their remarkable structural, electrical and optical properties, current experimental results show mobilities of ~50 $cm^2/V{\cdot}s$[13]. This significant discrepancy from theoretical predictions points to dominant scattering mechanisms that limit electrical conductivity, hindering their competitiveness with widely adopted electronic and optoelectronic materials such as Si and GaAs[14–22].

The successful deployment of TMD materials as active components in high-performance optoelectronic devices critically depends on the availability of both n-type and p-type doping. Due to the strong covalent bonds within each layer and their atomically thin structure, traditional doping techniques used for bulk semiconductors are not suitable for 2D materials, as they often cause significant structural damage or introduce deep-level defects. For instance, ion implantation can create disordered lattices, while high-temperature diffusion doping can lead to interlayer delamination or unintentional phase transitions. These effects severely degrade the optoelectronic performance by reducing carrier mobility, quenching photoluminescence, or increasing trap-assisted recombination[23–26]. On the other hand, due to the atomic thickness of TMDs, their optical and structural properties, as well as carrier dynamics, can be effectively engineered by using various post-growth methods[27–29]. While doping is necessary to inject carriers efficiently, it must be achieved without sacrificing the material's high excitonic emission efficiency. In this context, a critical balance must be struck. The key to fully unlocking the potential of TMDs in optoelectronics

[1]Department of Physics, Faculty of Science, Istanbul University, Vezneciler, Istanbul, 34134, Turkey. [2]Paul-Drude-Institute for Solid State Electronics, Leibniz Institute within Forschungsverbund Berlin eV., Hausvogteiplatz 5-7, 10117 Berlin, Germany. [3]Department of Physics Engineering, Istanbul Technical University, Maslak, Istanbul, 34467, Turkey. [4]School of Physics, Engineering and Technology, University of York, York, YO10 5DD, UK. ✉e-mail: yue.wang@york.ac.uk; fahrettin.sarcan@istanbul.edu.tr

lies in developing doping strategies that can simultaneously enhance carrier concentration while preserving bright excitonic photoluminescence.

Chemical treatment typically relies on surface adsorption or substitutional doping through reaction with precursor molecules. Ion implantation involves accelerating dopant ions into the material, allowing precise control but often causing lattice damage. Plasma doping introduces energetic ions or radicals that can modify the surface or embed dopants. Thermal annealing promotes the diffusion of dopants or activates existing ones by repairing defects. Electron beam irradiation induces defects or modulates local electronic structure through energy transfer, while ultraviolet-ozone treatment introduces oxygen-related species that chemically modify the surface or passivate defects[30–37]. The remaining challenge in post-growth doping of 2D materials lies in maintaining their excellent optical properties while consistently controlling the doping concentration. In this study, we specifically addressed this challenge in the context of chemical treatment based on 1,2-dichloroethane (DCE).

The chemical formula of DCE is $C_2H_4Cl_2$. When $MoS_2$ is submerged in DCE solution, chlorine (Cl) atoms interact with $MoS_2$, acting as electron donors and leaving behind ethylene gas ($C_2H_4$). It has been employed as an effective tool for defect engineering and doping in graphene and 2D TMDs. Several studies in the literature have demonstrated the n-type doping of TMDs using DCE solution. L. Yang et al. reported n-type doping in $WS_2$ and $MoS_2$ via a 12-hour DCE treatment, resulting in reduced contact resistance from ~$10^2$ kΩ·μm to 0.7 kΩ·μm and 0.5 kΩ·μm, respectively[38]. In a recent study by A. Roy et al., it is demonstrated that the Schottky barrier height of $WS_2$ decreased from 1.02 eV to 0.8 eV with a DCE treatment applied as a function of treatment time, from 6 to 24 h[39]. T.Y. Kim et al. proposed using varying molar concentrations of DCE solvent for improved control over the doping process in $MoS_2$[40]. They reported a well-defined correlation between carrier density and the molar concentration of DCE during a 45-minute treatment[40]. While the effects of the DCE treatment on the electrical properties of the aforementioned TMDs have been comprehensively studied and optimised by different research groups, its impact on the optical properties of TMDs remains unclear.

In this study, we systematically investigate the dependence of the optical properties of semiconducting TMDs on both DCE treatment time and layer number. We exfoliated $MoS_2$ flakes with different numbers of layers on polydimethylsiloxane (PDMS), from monolayer to bulk, and transferred the flakes to fused silica substrates. PL spectroscopy is carried out to investigate the effect on their optical properties with a wide range of DCE treatment durations. To elucidate the energetically favoured Cl-doping mechanisms in $MoS_2$ and the influence of intrinsic sulphur defects on its optical properties, density functional theory (DFT) calculations are performed.

## Results

### Structural and electrical characterisation

We prepared a series of $MoS_2$ samples on fused silica substrates using the scotch tape, PDMS-assisted mechanical exfoliation and deterministic transfer process (see **Methods**). The photoluminescence (PL) spectrum measured from the exfoliated flakes is utilised to confirm their number of layers both on the PDMS and fused silica substrate (see Figure S1). The peak value for monolayer $MoS_2$ occurs at approximately 655 nm, representing the direct bandgap. The indirect transition peak of bilayer $MoS_2$ starts to appear around 802 nm, while its direct transition peak is around 665 nm. From a monolayer to a thicker flake, the PL intensity dramatically decreases as a function of increased thickness, and the bandgap of $MoS_2$ red shifts up to 1.35 eV, i.e. 921 nm, as shown in the inset of Figure S2. However, distinguishing the indirect band gaps beyond 7 layers becomes challenging. We refer to more than 7-layer flakes as bulk flakes.

In the literature, T.Y. Kim et al. demonstrated that a 45-minute treatment effectively dopes $MoS_2$[40], while L. Yang et al. reported n-type doping in $WS_2$ and $MoS_2$ via a 12-hour DCE treatment[38], which reduced the contact resistance from ~102 kΩ·μm to 0.7 kΩ·μm and 0.5 kΩ·μm, respectively. These findings serve as reference points for this study. As a first step, we reproduced the reported doping effect via DCE treatment, characterised by Raman spectroscopy. By evaluating the electrical properties through the fabrication of a field-effect transistor (FET) based on a few-layer $MoS_2$. This validation ensured consistency with the literature before we focused on investigating the optical properties.

Raman spectroscopy was performed to confirm the n-type doping effect of DCE, see Methods. The first-order Raman spectra of multilayer (ML) $MoS_2$ exhibit two optical phonon modes: the $E^1_{2g}$ mode, which corresponds to in-plane vibrations of both the metal and chalcogen atoms, and the $A_{1g}$ mode, which corresponds to out-of-plane vibrations of the chalcogen atoms. It is well established that the $A_{1g}$ mode is highly sensitive to doping due to its strong coupling with electrons, whereas the $E^1_{2g}$ mode is more sensitive to strain and lattice distortions[41,42]. n-type doping typically induces a redshift and line broadening of the $A_{1g}$ peak, while p-type doping leads to a blueshift. Figure 1a shows the Raman spectra of pristine and 45-minute DCE-treated flakes. After the doping process, both vibrational modes shifted downward due to enhanced electron–phonon scattering in the n-doped $MoS_2$ flakes. Specifically, the $E^1_{2g}$ mode exhibited a shift of ~0.3 $cm^{-1}$, while the $A_{1g}$ mode shifted by ~1.1 $cm^{-1}$. This behaviour can be attributed to lattice contraction induced by chloride dopants[40]. The larger redshift of the $A_{1g}$ peak compared to the $E^1_{2g}$ peak is a clear indicator of the n-type doping effect.

For electrical characterisation, FET devices were fabricated on few-layer $MoS_2$ flakes using electron-beam lithography (details are included in the **Methods**). Optical microscope images of a few-layer $MoS_2$ FET device, output and transfer characteristics of the FET device before and after DCE treatment are shown in Fig. 1b–d. Electrical characterisations were done at room temperature in ambient atmosphere. The output characteristics show that the drain current increased up to 1.5 μA under a 1 V negative drain bias across a 3 μm channel length at 0 V gate voltage (Fig. 1c). According to the transfer characteristics of the 3 μm channel device, $I_{on}/I_{off}$ ratio of the pristine FET is 2 orders of magnitude and is improved to 6 orders of magnitude after 12 h of treatment (Fig. 1d). The pristine sample exhibits n-type characteristics[31], which are enhanced after 12 h in DCE solution.

### Optical characterisation

The PL spectra of different layers are characterised before and after 2-minute and 60-minute DCE treatment (Fig. 2), see Methods. After 60 min in the DCE solution, the PL peak intensity of monolayer $MoS_2$ decreases to ~80% of its initial value. Under the same treatment time, the PL peak intensity of the direct transition in bilayer (2 L) $MoS_2$ retains 70 ± 15% of its initial intensity, while the indirect transition retains only 18 ± 11%. Repeated 60-minute DCE treatments show a layer-dependent response, where the suppression of the indirect transition diminishes with increasing thickness. The same experiments are repeated with the pristine flakes for 2 min of DCE treatment, and it is observed that even with 2 min of treatment time, the PL intensity of the indirect transition for 2 L and beyond reduces significantly, while their direct transition intensity remains almost unaffected. A more in-depth analysis of the direct bandgap emission is carried out by employing a multi-peak fitting to separate the exciton and trion emission, see Figure S3 in Supplementary Information. The trion contribution increases with the number of layers, while the exciton intensity decreases. This behaviour can be explained by the doping effect of DCE. In thicker layers, the conduction band edge shifts closer to the localised Cl-defect energy levels, thereby favouring the trion formation.

The same DCE treatment is processed on more than a hundred samples with various layer numbers and under different time durations. Figure 3 shows the overview of the PL ratios of DCE-treated to pristine $MoS_2$ samples for both direct and indirect transitions of 1 L (direct only), 2 L, 4 L, 6 L, 7 L, and bulk, over periods ranging from 30 seconds to 24 h. The effect of DCE treatment on the PL intensity of 2D $MoS_2$ is assessed for each flake individually by taking the ratio of the peak intensities, R, before and after treatment ($R = I_{dope}/I_{pristine}$). The data points with error bars in Figs. 3 and 4 represent the average values of R for all (>100) samples exposed to the same duration in the DCE solution. It is clear that the impact of DCE treatment is

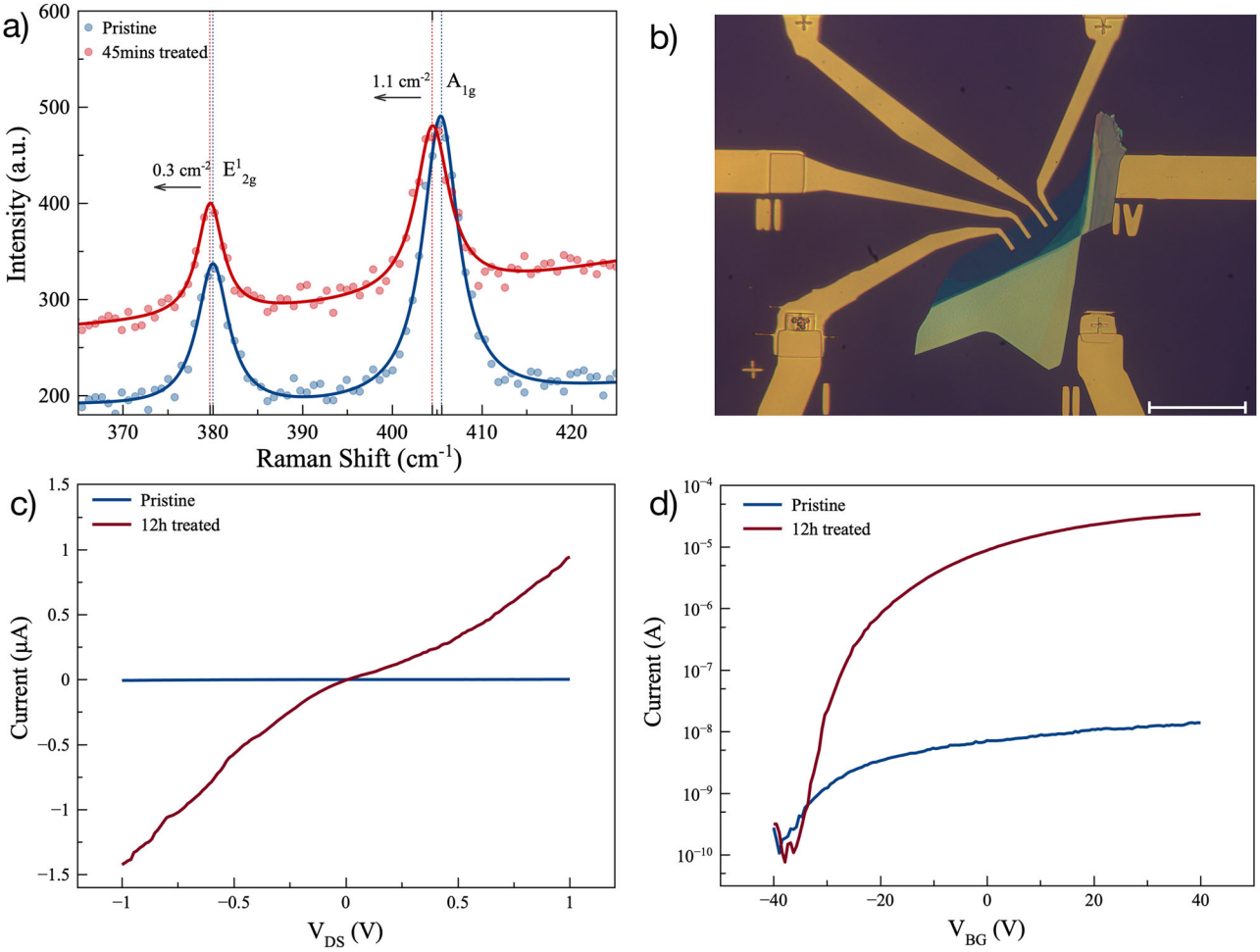


**Fig. 1 | N-type doping in 5-layer $MoS_2$ via DCE treatment. a** Raman spectra of 5-layer $MoS_2$ before and after a 45-minute DCE treatment; **b** optical microscope image with a scale bar of 50 μm; **c** output and **d** transfer characteristics of the field-effect transistor (FET) device before and after a 12h DCE treatment.

not the same on the direct and indirect transitions of $MoS_2$ samples, i.e. the indirect transitions are affected more than the direct transitions for all layers. In other words, the indirect transitions in the multilayer $MoS_2$ can be damped, while the direct transition is maintained.

The effect of DCE on the optical properties of $MoS_2$, under the same treatment time, also depends on the number of layers. Figure 4 shows the intensity ratio R as a function of the number of layers for different doping durations. The impact of DCE on the PL intensity across all treatment durations reduces as the number of layers increases. The layer dependency of DCE treatment in $MoS_2$ flakes eventually saturates. The dashed line fittings are guides to the eye to highlight the difference in the effect between the direct and indirect transitions. This trend may indicate that the doping process affects only the surface layers.

### Density functional theory calculation

To understand the mechanisms behind the n-type doping and optical changes observed after DCE treatment, we used DFT to calculate the most energetically favourable adsorption sites for chlorine (more details on the model are included in **Methods**). We also computed the electronic band structures and density of states (DOS) for both pristine monolayer and bilayer $MoS_2$ to determine the most probable interaction scenario. Figure 5 shows the energetic preference of symmetry-permitted doping sites for Cl in $MoS_2$, where the defect formation ($E_{vac}$), Cl binding ($E_{ads}$), and total formation ($E_{form}$) energies, are indicated with orange, blue and green bars. The DFT calculations show that the Cl binding at an interstitial site of a $MoS_2$ lattice is energetically highly endothermic (7 eV for H3, Fig. 5d), while one adsorbed on S-vacancy is exothermic, meaning that Cl binding to defects is an energetically driven process (-1.9 eV for both T3 and B3, Fig. 5b, c). Even with a preceding defect formation in a pristine $MoS_2$, the total energy required for substitutional doping of Cl for an S atom is still lower (1.8 eV for both T3 and B3) than those for interstitial doping (H3 and vdW gap, Fig. 5e). When comparing the total formation energies, Cl adsorption on a pristine surface is energetically most favourable (0.9 eV for T1) – which is the essential step to attract Cl to the surface (Fig. 5a). This is followed by the energies for the replacement of a surface S atom by a Cl atom in T3 and B3 models. Cl doping at the vdW gap (VDG in Fig. 5e), is energetically more expensive than substitutional doping, while cheaper than the interstitial doping.

These results indicate that the most likely scenario is that the Cl atoms are filling the S-vacancies or replacing S atoms in $MoS_2$ during the doping process. Moreover, the DFT results suggest that, depending on the local chemical environment and doping conditions, it is also likely for Cl atoms to migrate at the vdW gap in the $MoS_2$ multilayers – this indeed increases the interlayer spacing while reducing the interlayer coupling, which can alter the electronic band structure of $MoS_2$.

The band structure analysis in Fig. 6 highlights the effect of treatment on the electronic band structure of materials. The PBE-calculated bandgap of monolayer $MoS_2$ is smaller than the experimental value (~1.8 - 1.9 eV). This result is consistent with the known underestimation of bandgaps by semi-local functionals, but does not impact our analysis of the doping mechanism. In the presence of substitutional doping of Cl in a bilayer $MoS_2$, the bandgap still exhibits indirect bandgap characteristics with a narrower bandgap (Fig. 6c, d) compared to the pristine layer (Fig. 6a, b) while the insertion of Cl at the vdW gap, i.e. VDG, causes less dispersive (flatter) bands

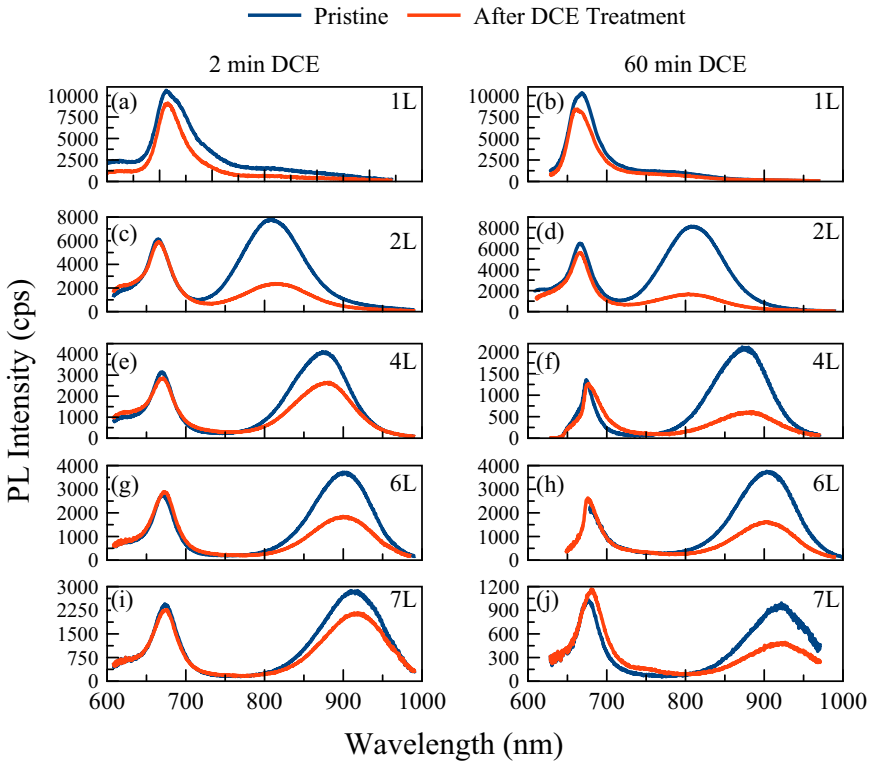


**Fig. 2 | Photoluminescence spectra of monolayer to multilayer $MoS_2$ under DCE treatment.** PL spectra of (**a**, **b**) 1 L, (**c**, **d**) 2 L, (**e**, **f**) 4 L, (**g**, **h**) 6 L, and (**i**, **j**) 7 L $MoS_2$ flakes measured before (dark blue) and after (orange) exposure to DCE solution for 2 min (left column) and 60 min (right column).

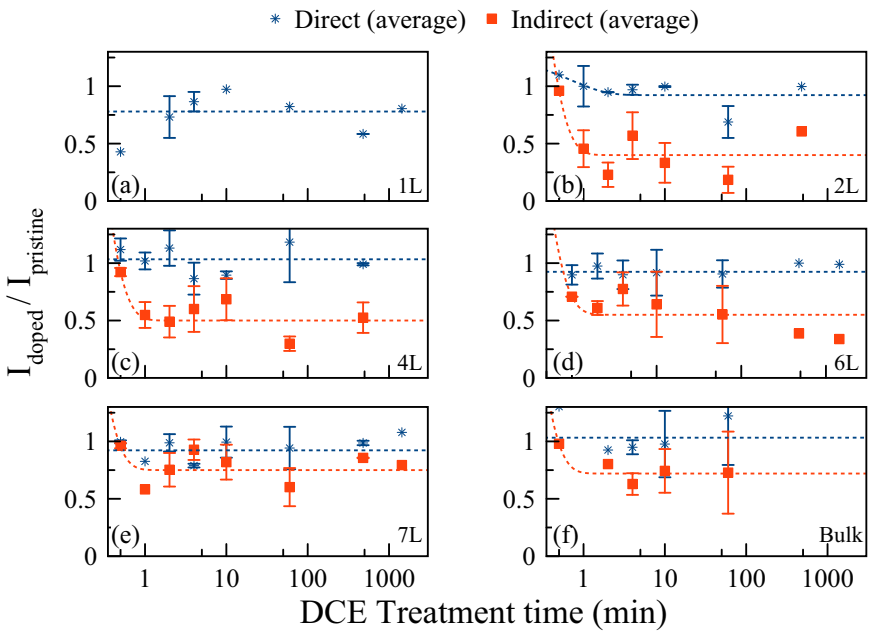


**Fig. 3 | Time-dependent evolution of direct and indirect excitonic emissions in DCE-treated $MoS_2$.** Time dependence of the PL intensity ratios before and after DCE treatment for both direct (dark blue) and indirect (orange) transitions of (**a**) 1 L, (**b**) 2 L, (**c**) 4 L, (**d**) 6 L, (**e**) 7 L, and (**f**) bulk $MoS_2$, plotted as a function of treatment duration in logarithmic scale from 30 s to 1440 min (24 h).

resulting in both lowering the bandgap and transition from indirect to direct bandgap (Fig. 6e).

Density-of-state (DOS) calculations give additional support to our hypothesis and reveal the effect of dopant contribution near the Fermi level energy states (Fig. 6f–h). This leads to an increase in electrical conductivity. The emergence of an additional nearly flat band around the Fermi energy level indicates strong electronic localisation due to the VDG dopant (Fig. 6e, h). Also, the indirect bandgap feature significantly diminishes upon vdW gap doping, compared to the substitutional doping in T3 and B3 models (Fig. 6c, d, g). This suggests, while both substitutional and interstitial doping are likely to suppress the indirect bandgap feature as observed in experiments, the vdW gap type doping is likely to induce the bandgap transition. All these results together indicate that Cl-doping is a candidate mechanism for engineering the bandgap.

Chlorine (Cl) atoms are found to settle at defect sites near the $MoS_2$ indirect band level. This facilitates non-radiative relaxation from the conduction to the valence band, thereby quenching the PL intensity of the indirect transition. We attribute the unaffected direct transition to its occurrence solely at the K-point, which is relatively isolated in momentum space and thus less sensitive to defect-induced scattering or trapping. Defects arising from Cl-doping introduce localised states that primarily

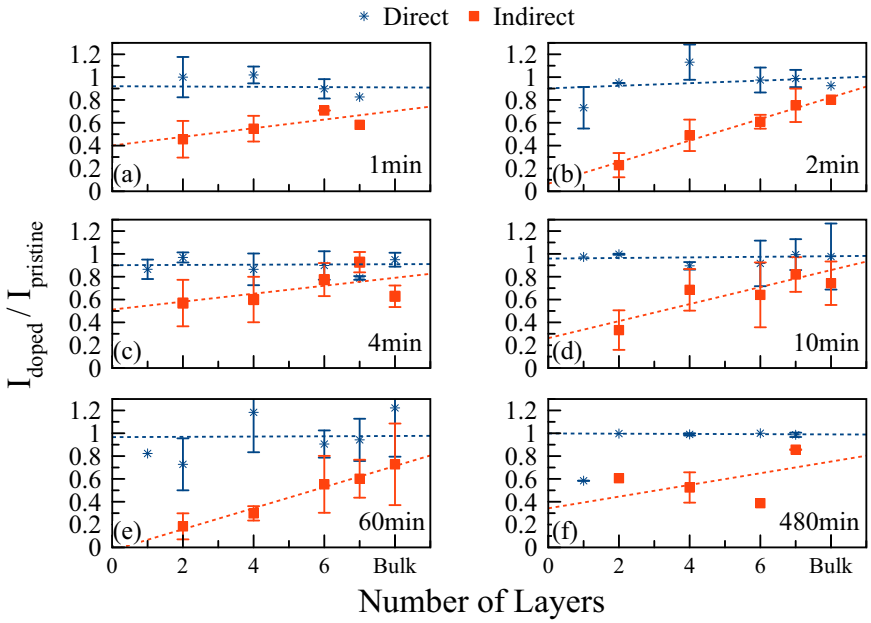


**Fig. 4 | Layer-dependent evolution of $MoS_2$ under different DCE treatment durations.** $MoS_2$ layer dependence of the PL intensity ratios before and after DCE treatment in both direct (dark blue) and indirect (orange) transitions, with (**a**) 1 min, (**b**) 2 min, (**c**) 4 min, (**d**) 10 min, (**e**) 60 min and (**f**) 480 min DCE treatment.

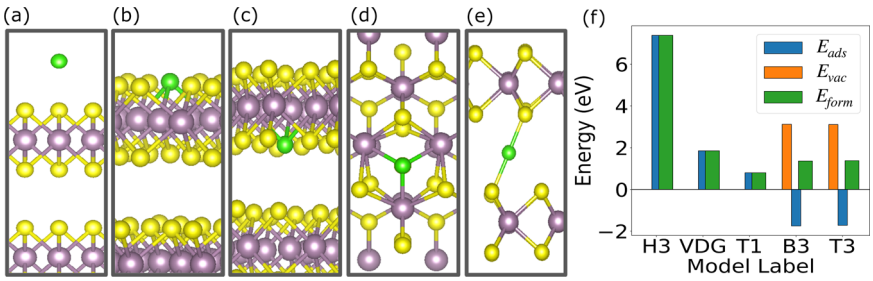


**Fig. 5 | Atomic configurations and formation energy analysis of Cl-doped bilayer $MoS_2$.** Optimised configurations of a $MoS_2$ bilayer with Cl (**a**) adsorbed on the surface (T1), **b** replacing a S atom on the upper S (T3) and **c** the lower S layer of $MoS_2$ (B3), **d** inserted at the centre of honeycomb neighbouring by three Mo atoms (H3) and **e** inserted at the vdW gap. **f** A graph depicting S-vacancy formation energy $E_{form}$, which is the sum of $E_{vac}$ and $E_{ads}$, along with $E_{vac}$ and $E_{ads}$.

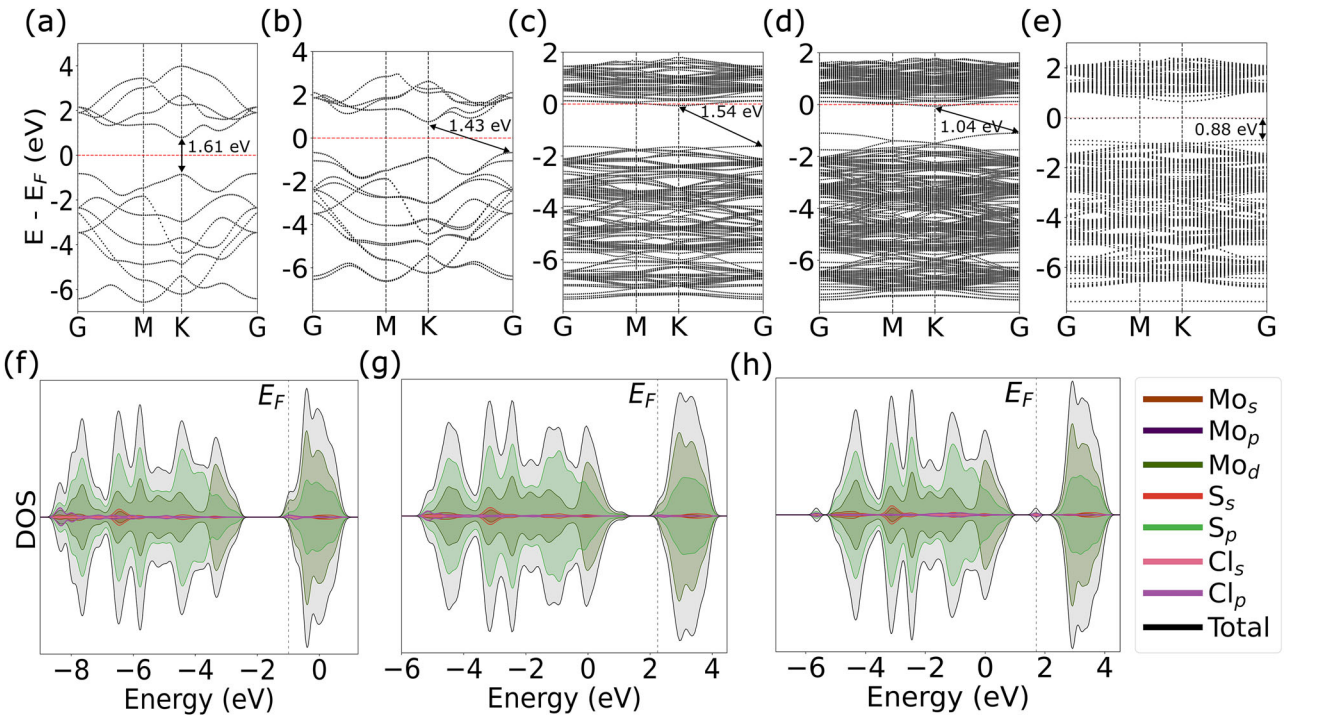


**Fig. 6 | Electronic band structure and density of states of pristine and Cl-doped $MoS_2$.** DFT computed electronic bandgap structures of a pristine (**a**) monolayer and (**b**) bilayer $MoS_2$; and a bilayer $MoS_2$ with Cl doped on (**c**) T3, **d** B3 and (**e**) at the vdW gap. Density of state (DOS) calculations of (**f**) a pristine bilayer, Cl-doped on (**g**) T3 and (**h**) at the vdW gap.

affect extended states across the band structure, leaving the highly localised direct transition largely unaffected.

## Discussion

This work addresses a critical trade-off, which is the need to electrically dope the material without sacrificing its bright excitonic emission, in developing optoelectronic devices from 2D TMDs. While doping is essential for efficient charge injection in devices like LEDs and lasers, many methods degrade the optical quality. Through comprehensive photoluminescence characterisation, a suppression in the indirect transition peak intensity was observed, even after short 1,2-dichloroethane (DCE) exposures (i.e., 2 min), while the direct transition remained largely unaffected across all layer numbers. This effect was more pronounced with increased treatment duration and diminishes with increased layer thickness, indicating a layer- and time-dependent doping behaviour.

Density functional theory calculations revealed that chlorine atoms preferentially occupy sulphur vacancy sites in $MoS_2$, forming energetically favourable configurations. These Cl dopants introduce in-gap states near the conduction band edge, promoting non-radiative recombination pathways that selectively reduce the indirect PL transitions.

The key importance of this study is the demonstration that DCE treatment can selectively suppress the inefficient indirect bandgap emission while preserving the efficient direct excitonic transition. Given that this effect is driven by the interaction between chlorine and common chalcogen vacancies, this bandgap engineering strategy is likely applicable to other semiconducting TMDs, such as $WS_2$, $WSe_2$ and $MoTe_2$. Such capability represents a powerful form of bandgap engineering, as it effectively removes a competing non-radiative pathway and enhances the relative contribution of the desired light-emitting channel. By transforming a material to have a more pronounced direct-gap character, this method paves the way for creating TMD-based light emitting devices with significantly improved efficiency.

In summary, we systematically investigated the impact of chlorine-based chemical treatment using 1,2-dichloroethane on the optical properties of two-dimensional $MoS_2$ with varying layer numbers and treatment durations. Our insight suggests a transition from an indirect to direct bandgap character in multilayer $MoS_2$, effectively enabling bandgap engineering through surface chemical doping. It is demonstrated that the DCE treatment is a tuneable post-growth strategy, not only for n-type doping but also for manipulating the optical response of $MoS_2$. The ability to selectively suppress indirect transitions while maintaining the integrity of direct transitions provides a powerful strategy for enhancing excitonic emission in TMD-based optoelectronic devices, particularly in applications where robust direct-gap emission is crucial.

## Methods

### Sample preparation

Bulk single-crystal $MoS_2$ are purchased from HQ Graphene and 2D Semiconductors, which are slightly n-type in their pristine state (see field effect transistor characterisations given in supplementary material)[31]. The Scotch tape and PDMS-assisted mechanical exfoliation method is used to obtain $MoS_2$ flakes with different numbers of layers[43]. Flakes larger than 10 × 10 µm are transferred onto fused silica substrates using a custom-built viscoelastic transfer system. In the first stage of the study, the number of layers in the flakes was determined using AFM, PL, and an image-processing-based method[44] (see Figure S1). For $MoS_2$, a well-studied material, PL offers a faster and more reliable approach compared to AFM. Therefore, PL is mostly used in this study.

### Raman and photoluminescence spectroscopy

The Raman and photoluminescence (PL) spectra of the flakes are measured using a custom-built modular micro spectroscopy setup equipped with a 500 mm monochromator (Shamrock 500i, Andor), a Si CCD (Newton BEX2-DD, Andor) and a 532 nm excitation laser, before and after DCE treatment. The laser power was kept constant at 2 mW with an integration time of 1 s for all the PL measurements, whereas Raman measurements were performed with a laser power of 10 mW and an integration time of 10 s. The laser beam is focused to a spot of ~0.8 µm in diameter with a 100x objective (numerical aperture, NA = 0.7). After obtaining PL measurements for pristine flakes, the samples are soaked in the DCE solution for varying durations, ranging from 30 seconds to 24 h, in a clean room atmosphere. Immediately after DCE treatment, the flakes are dried with $N_2$ gas. Finally, PL measurements are conducted on DCE-treated samples at room temperature. For each sample, the intensity ratio of the PL peaks before and after DCE treatment is calculated to assess the effect of the DCE treatment.

### Fabrication and characterisation of field effect transistor

For electrical characterisation, the flake is transferred onto the $SiO_2$ (300 nm)-on-Si substrate, which is cleaned with acetone (ACE) and isopropyl alcohol (IPA) before the transfer process. The electrodes are patterned on the sample by electron-beam lithography (EBL) with a bilayer resist to obtain an undercut structure (MMA/PMMA, Allresist GmbH). Au/Cr (60 nm/10 nm) is deposited as contact electrodes. The lift-off process is carried out in warm ACE. The fabricated FET device is mounted onto a ceramic chip holder with wires bonded for electrical characterisation. Electrical characterisation is carried out on the FET devices before and after 12 h of DCE treatment. Output and transfer characterisations are measured using an Agilent B2902A source measure unit at room temperature.

### Computational methods

DFT calculations are conducted using the Quantum Espresso software package[45,46], to unveil the complex interplay between $MoS_2$ and the Cl-doping process. The projected augmented wave pseudo-potentials[47,48] and the Perdew–Burke–Ernzerhof parametrisation of the generalised gradient approximation exchange-correlation functional are employed[49]. Although PBE is well known to underestimate semiconductor band gaps due to the self-interaction error, it remains widely employed because of its computational efficiency[50–52]. In this work, we use PBE primarily to capture relative trends in defect states, rather than to provide a quantitative prediction of the absolute band gap. A $6 \times 6 \times 1$ K-point mesh within the Gamma-centred Monkhorst-Pack scheme is applied to Brillouin Zone integration with a kinetic energy cut-off of 60 Ry and a density cut-off of 480 Ry. A Gaussian smearing scheme is utilised with a broadening of 0.01 Ry. In the geometry optimisations, the system is allowed to relax fully using a Broyden–Fletcher–Goldfarb–Shanno (BFGS) algorithm along with the total energy threshold of $10^{-5}$ Ry and the force threshold of $10^{-3}$ Ry/Å.

The defect calculations were performed in a 4×4 supercell (48 atoms), corresponding to an effective defect–defect separation of ~12.74 Å. This setup yields a defect concentration of 7.1 $10^{13}$ $cm^{-2}$, which is higher than in high-quality exfoliated samples[53,54]. but falls within the range reported for CVD-grown or irradiated films[55,56]. Additionally, the 4×4 cell size is a widely adopted compromise in defect studies of 2D materials, balancing the need to minimize spurious defect interactions with the steep computational cost of larger supercells. We adopted six defect models:two substitutional and four interstitial doping models. In substitutional doping models of T3 and B3, an isolated Cl atom substitutes for an S atom on either the upper (T3) or the lower S layer (B3) of $MoS_2$. Note that, in the substitutional doping models, metal vacancies are not considered as their formation is energetically highly unfavourable[57]. In the interstitial doping models, an isolated Cl atom is introduced via interstitial insertion at different symmetry-allowed sites: T1, H3, and the van der Waals (vdW) gap within the $MoS_2$ lattice. T1 is a one-fold coordinated site on the topmost Mo atom. H3 is a three-fold coordinated site at the centre of the honeycomb formed by three Mo atoms. VdW gap site is a one-fold coordinated site at the vdW gap of a $MoS_2$ bilayer.

Substitutional doping process (i.e. T3 and B3) mainly consists of two elementary steps: (i) a vacancy formation in $MoS_2$ after the immersion in a solution, leading to the generation of dangling bonds, and (ii) chemical adsorption of Cl on $MoS_2$. The formation energy associated with Cl doping, $E_{form}$ can be computed as a sum of vacancy formation energy, $E_{vac}$, and

adsorption energy of Cl, $E_{ads}$.

$$E_{form} = E_{vac} + E_{ads} \quad (1)$$

$$E_{ads} = E_{doped} + (E_{system} + \eta_{Cl} \times \mu_{Cl}) \quad (2)$$

where $E_{doped}$ is the total energy of a Cl-doped $MoS_2$ system, $\eta_{Cl}$ is the number of Cl atoms doped in $MoS_2$ and $\mu_{Cl}$ is the chemical potential of a Cl atom in a $Cl_2$ gas molecule. For the interstitial doping models, the Cl adsorption energy is computed using only Eq. 2.

$$E_{vac} = E_{system} - (E_{pristine} - \eta_s \times \mu_s) \quad (3)$$

where $E_{system}$ and $E_{pristine}$ are the total energies of a $MoS_2$ sheet with and without vacancy, respectively. $\eta_S$ is the number S atoms removed from the sheet and $\mu_s$ is the chemical potential of a S atom, referenced to the energy per atom in α-S bulk.

Following full relaxation, density of states and electronic band calculations are performed on the most energetically favourable model. The models depicted in the figures are visualised using VESTA software[58].

## Data availability

The authors declare that all the data supporting the findings of this study are available within the article or upon request from the corresponding author.

## Code availability

The authors declare that all the code supporting the findings of this study are available within the article or upon request from the corresponding author.

Received: 25 July 2025; Accepted: 12 November 2025;
Published online: 30 November 2025

## References

1. Wang, J., Han, J., Chen, X. & Wang, X. Design strategies for two-dimensional material photodetectors to enhance device performance. *InfoMat.* **1**, 33–53 (2019).
2. Manzeli, S., Ovchinnikov, D., Pasquier, D., Yazyev, O. V. & Kis, A. 2D transition metal dichalcogenides. *Nat, Rev. Mater.* **2**, 17033 (2017).
3. Jariwala, D., Sangwan, V. K., Lauhon, L. J., Marks, T. J. & Hersam, M. C. Emerging device applications for semiconducting two-dimensional transition metal dichalcogenides. *ACS Nano* **8**, 1102–1120 (2014).
4. Fiori, G. et al. Electronics based on two-dimensional materials. *Nat. Nanotechnol.* **9**, 768–779 (2014).
5. Kuş, E. et al. A Dual-Channel MoS2-Based Selective Gas Sensor for Volatile Organic Compounds. *Nanomaterials* **14**, 1–13 (2024).
6. Radisavljevic, B., Radenovic, A., Brivio, J., Giacometti, V. & Kis, A. Single-layer MoS2 transistors. *Nat. Nanotechnol.* **6**, 147–150 (2011).
7. Wang, Q. H., Kalantar-Zadeh, K., Kis, A., Coleman, J. N. & Strano, M. S. Electronics and optoelectronics of two-dimensional transition metal dichalcogenides. *Nat. Nanotechnol.* **7**, 699–712 (2012).
8. Chae, W. H., Cain, J. D., Hanson, E. D., Murthy, A. A. & Dravid, V. P. Substrate-induced strain and charge doping in CVD-grown monolayer MoS2. *Appl Phys. Lett.* **111**, 143106 (2017).
9. Qiu, H. et al. Electrical characterization of back-gated bi-layer MoS 2 field-effect transistors and the effect of ambient on their performances. *Appl Phys. Lett.* **100**, 123104 (2012).
10. Baugher, B. W. H., Churchill, H. O. H., Yang, Y. & Jarillo-Herrero, P. Intrinsic electronic transport properties of high-quality monolayer and bilayer MoS2. *Nano Lett.* **13**, 4212–4216 (2013).
11. Armstrong, A., McKenna, K. P. & Wang, Y. Directional dependence of band gap modulation via uniaxial strain in MoS2 and TiS3. *Nanotechnology.* **35**, 015704 (2023).
12. Splendiani, A. et al. Emerging photoluminescence in monolayer MoS2. *Nano Lett* **10**, 1271–1275 (2010).
13. Larentis, S., Fallahazad, B. & Tutuc, E. Field-effect transistors and intrinsic mobility in ultra-thin MoSe 2 layers. *Appl. Phys. Lett.* **101**, 223104 (2012).
14. Wang, H. et al. Integrated circuits based on bilayer MoS 2 transistors. *Nano Lett.* **12**, 4674–4680 (2012).
15. Liu, H. et al. Switching mechanism in single-layer molybdenum disulfide transistors: An insight into current flow across Schottky barriers. *ACS Nano* **8**, 1031–1038 (2014).
16. Liu, W. et al. Role of metal contacts in designing high-performance monolayer n-type WSe2 field effect transistors. *Nano Lett.* **13**, 1983–1990 (2013).
17. Das, S., Chen, H. Y., Penumatcha, A. V. & Appenzeller, J. High performance multilayer MoS2 transistors with scandium contacts. *Nano Lett.* **13**, 100–105 (2013).
18. Walia, S. et al. Characterization of metal contacts for two-dimensional MoS2 nanoflakes. *Appl. Phys. Lett.* **103**, 232105 (2013).
19. Kang, J., Liu, W. & Banerjee, K. High-performance MoS2 transistors with low-resistance molybdenum contacts. *Appl. Phys. Lett.* **104**, 093106 (2014).
20. Liu, H., Neal, A. T., Du, Y. & Ye, P. D. Defect-DOMINATED DOPING and CONTACTRESISTANCE in MoS2. *ACS Nano* **8**, 2880–2888 (2014).
21. Liu, D., Guo, Y., Fang, L. & Robertson, J. Sulfur vacancies in monolayer MoS2 and its electrical contacts. *Appl. Phys. Lett.* **103**, 183113 (2013).
22. McDonnell, S., Addou, R., Buie, C. & Wallace, R. M. & Hinkle, C. L. Defect-DOMINATED DOPING and CONTACT RESISTANCE in MoS2. *ACS Nano* **8**, 2880–2888 (2014).
23. Loh, L., Zhang, Z., Bosman, M. & Eda, G. Substitutional doping in 2D transition metal dichalcogenides. *Nano Res.* **14**, 1668–1681 (2021).
24. Wang, Y., Zheng, Y., Han, C. & Chen, W. Surface charge transfer doping for two-dimensional semiconductor-based electronic and optoelectronic devices. *Nano Res.* **14**, 1682–1697 (2021).
25. Luo, P. et al. Doping engineering and functionalization of two-dimensional metal chalcogenides. *Nanoscale Horizons* **4**, 26–51 (2019).
26. Pham, V. P. & Yeom, G. Y. Recent advances in doping of molybdenum disulfide: industrial applications and future prospects. *Adv. Mater.* **28**, 9024–9059 (2016).
27. Qu, D. et al. Carrier-type modulation and mobility improvement of thin MoTe2. *Adv. Mater*. **29**, (2017).
28. Miao, J. et al. A 'click' Reaction to Engineer MoS2Field-effect transistors with low contact resistance. *ACS Nano* **16**, 20647–20655 (2022).
29. Liu, K. et al. Approaching ohmic contact to two-dimensional semiconductors. *Sci. Bull.* **64**, 1426–1435 (2019).
30. Sarcan, F. et al. Understanding the impact of heavy ions and tailoring the optical properties of large-area monolayer WS2 using focused ion beam. *NPJ 2D Mater. Appl.* **7**, 23 (2023).
31. Sarcan, F. et al. Ultraviolet-ozone treatment: an effective method for fine-tuning optical and electrical properties of suspended and substrate-supported MoS2. *Nanomaterials* **13**, 3034 (2023).
32. Luo, T. et al. Electron beam lithography induced doping in multilayer MoTe2. *Appl. Surf. Sci.* **540**, 148276 (2021).
33. Amani, M. et al. High luminescence efficiency in MoS2 grown by chemical vapor deposition. *ACS Nano* **10**, 6535–6541 (2016).
34. Iqbal, M. W., Elahi, E., Amin, A., Hussain, G. & Aftab, S. Chemical doping of transition metal dichalcogenides (TMDCs) based field effect transistors: A review. *Superlattices Microstruct.* **137**, 106350 (2020).
35. Choi, M. S., Lee, M., Ngo, T. D., Hone, J. & Yoo, W. J. Chemical dopant-free doping by annealing and electron beam irradiation on 2D materials. *Adv Electron Mater* **7**, (2021).
36. Neupane, G. P. et al. Simple Chemical Treatment to n-Dope Transition-Metal Dichalcogenides and Enhance the Optical and

Electrical Characteristics. *ACS Appl Mater. Interfaces* **9**, 11950–11958 (2017).
37. Kim, Y. et al. Plasma functionalization for cyclic transition between neutral and charged excitons in monolayer MoS2. *Sci Rep* **6**, (2016).
38. Yang, L. et al. Chloride molecular doping technique on 2D materials: WS2 and MoS2. *Nano Lett* **14**, 6275–6280 (2014).
39. Roy, A., Sharma, S. & Mondal, B. Effect of n-type Cl doping on electrical conductivity of few layer WS2. *Microsyst. Technol.* **31**, 1121–1131 (2025).
40. Kim, T., Kim, Y. & Kim, E. K. Characteristics of Cl-doped MoS2 field-effect transistors. *Sens. Actuators A Phys*. **312**, (2020).
41. Peimyoo, N. et al. Chemically driven tunable light emission of charged and neutral excitons in monolayer WS2. *ACS Nano* **8**, 11320–11329 (2014).
42. Iqbal, M. W., Shahzad, K., Akbar, R. & Hussain, G. A review on Raman finger prints of doping and strain effect in TMDCs. *Microelectron. Eng.* **219**, 111152 (2020).
43. Novoselov, K. S. et al. Two-dimensional atomic crystals. *Proc. Natl Acad. Sci. USA* **102**, 10451–10453 (2005).
44. Meriç, B. B., Erol, A. & Sarcan, F. A novel method to determine the layer number of 2D TMD materials based on optical microscopy and image processing. *Phys Scr.* **100**, (2025).
45. Giannozzi, P. et al. QUANTUM ESPRESSO: A modular and open-source software project for quantum simulations of materials. *J. Phys. Condens. Matter.* **21**, (2009).
46. Giannozzi, P. et al. Advanced capabilities for materials modelling with Quantum ESPRESSO. *J. Phys. Condens. Matter.* **29**, (2017).
47. Kresse, G. & Joubert, D. From ultrasoft pseudopotentials to the projector augmented-wave method. *Phys. Rev. B* **59**, 1758–1775 (1999).
48. Blöchl, P. E., Först, C. J. & Schimpl, J. The Projector Augmented Wave Method: Ab-Initio Molecular Dynamics with Full Wave Functions. *Bull. Mater. Sci.* **26**, 33–41 (2003).
49. Perdew, J. P., Burke, K. & Ernzerhof, M. Generalized gradient approximation made simple. *Phys. Rev. Lett.* **77**, 3865–3868 (1996).
50. Mori-Sánchez, P., Cohen, A. J. & Yang, W. Localization and delocalization errors in density functional theory and implications for band-gap prediction. *Phys. Rev. Lett.* **100**, 146401 (2008).
51. Perdew, J. P. & Levy, M. Physical content of the exact Kohn-Sham orbital energies: band gaps and derivative discontinuities. *Phys. Rev. Lett.* **51**, 1884–1887 (1983).
52. Sham, L. J. & Schlüter, M. Density-functional theory of the energy gap. *Phys. Rev. Lett.* **51**, 1888–1891 (1983).
53. Picker, J., Gan, Z., Neumann, C., George, A. & Turchanin, A. Low defect density in MoS2 monolayers grown on Au(111) by metal-organic chemical vapor deposition. *Micron* **186**, 103708 (2024).
54. Hossen, M. F., Shendokar, S., Khan, Md. A. R. & Aravamudhan, S. Quantitative Defect Analysis in CVD-Grown Monolayer MoS 2 via In-Plane Raman Vibration. *Nano Select* **6**, (2025).
55. Zhu, Y. et al. Room-temperature photoluminescence mediated by sulfur vacancies in 2D molybdenum disulfide. *ACS Nano* **17**, 13545–13553 (2023).
56. Zhang, X. et al. Low-defect-density monolayer MoS2 wafer by oxygen-assisted growth-repair strategy. *Adv. Sci.* **11**, e2408640 (2024).
57. Ostadhossein, A. et al. ReaxFF reactive force-field study of molybdenum disulfide (MoS2). *J. Phys. Chem. Lett.* **8**, 631–640 (2017).
58. Momma, K. & Izumi, F. VESTA 3 for three-dimensional visualization of crystal, volumetric and morphology data. *J. Appl Crystallogr* **44**, 1272–1276 (2011).

## Acknowledgements

This study was supported by the Scientific Research Projects Coordination Unit of Istanbul University, project numbers FBA-2023-39412 and FYL-2023-39742, and the Scientific and Technological Research Council of Turkey, project number 121F169. Y.W. acknowledges a Research Fellowship awarded by the Royal Academy of Engineering RF/201718/17131 and an EPSRC grant EP/V047663/1. C.S. and N.N. acknowledge the EuroHPC Joint Undertaking for awarding this project access to the EuroHPC supercomputer LEONARDO-BOOSTER, hosted by CINECA (Italy) and the LEONARDO consortium through an EuroHPC Benchmark Access call (EHPC-BEN-2024B11-048). They also thank the National Centre for High-Performance Computing (UHEM/ITU) (https://en.uhem.itu.edu.tr/) for the provision of additional computational resources under the grant number 1016652023. The authors would like to thank Dr. Alexander Armstrong and Prof. Keith McKenna for their valuable discussions on DFT.

## Author contributions

Y.K.B., E.H. and F.S. fabricated the samples, performed the Raman measurements, steady-state photoluminescence measurements and FET characterisation; C.S. performed the DFT calculations and was supervised by N.N; Y.K.B., N.N., A.E., Y.W. and F.S., analysed the results; A.E., Y.W and F.S. managed various aspects and funded the project; Y.K.B., and F.S. wrote the manuscript with contributions from all co-authors; Y.W. and F.S. oversaw the entire project. All authors have read and agreed to the published version of the manuscript.

## Competing interests

The authors declare no competing interests.

## Additional information

**Supplementary information** The online version contains supplementary material available at https://doi.org/10.1038/s41699-025-00639-0.

**Correspondence** and requests for materials should be addressed to Yue Wang or Fahrettin Sarcan.